

circMELK promotes glioblastoma multiforme cell tumorigenesis through the miR-593/EphB2 axis

Fengqi Zhou,^{1,5} Binbin Wang,^{1,5} Hong Wang,^{2,5} Lang Hu,^{1,5} Junxia Zhang,¹ Tianfu Yu,³ Xiupeng Xu,¹ Wei Tian,¹ Chunsheng Zhao,¹ Haifeng Zhu,⁴ and Ning Liu¹

¹Department of Neurosurgery, The First Affiliated Hospital of Nanjing Medical University, Nanjing 210029, Jiangsu Province, China; ²Department of Neurosurgery, Zhongda Hospital, School of Medicine, Southeast University, Nanjing 210029, Jiangsu Province, China; ³Department of Neurosurgery, The Affiliated Hospital of Nanjing University Medical School, Nanjing 210029, Jiangsu Province, China; ⁴Department of Neurosurgery, Funing Hospital, Funing 224400, Jiangsu Province, China

A number of studies indicate that circular RNAs (circRNAs) play paramount roles in regulating the biological behavior of glioblastoma multiforme (GBM). In this study, we investigated the underlying mechanism of circMELK in GBM. Real-time PCRs were used to examine the expression of circMELK in glioma tissues and normal brain tissues (NBTs). Localization of circMELK in GBM cells was estimated by fluorescence *in situ* hybridization (FISH). Transwell migration and three-dimensional invasion assays were performed to examine glioma cell migration and invasion *in vitro*. Spheroid formation, clonogenicity, and cell viability assays were implemented to test the stemness of glioma stem cells (GSCs). The functions of circMELK *in vivo* were investigated in a xenograft nude-mouse model. We have proved that circMELK functions as a sponge for tumor suppressor microRNA-593 (miR-593) by RNA immunoprecipitation and circRNA precipitation assays, which targets the oncogenic gene Eph receptor B2 (EphB2). Dual-luciferase reporter assays were adopted to estimate the interactions between miR-593 and circMELK or EphB2. We demonstrated that circMELK was upregulated in GBM, acting as an oncogene and regulating GBM mesenchymal transition and GSC maintenance via sponging of miR-593. Furthermore, we found that EphB2 was involved in circMELK/miR-593 axis-induced GBM tumorigenesis. This function opens the opportunity for the development of a novel therapeutic target for the treatment of gliomas.

INTRODUCTION

Glioblastoma multiforme (GBM), also known as the WHO grade IV glioma, is the most prevalent and malignant primary intrinsic brain tumor.¹ Despite recent advances in comprehensive therapeutics, including surgical resection followed by temozolomide chemotherapy and radiation treatment, the average survival after diagnosis is currently slightly over 1 year.^{2,3} The relapse of GBM after surgical resection is mainly due to the stem-cell-like properties of a small number of cells, which are called glioma stem cells (GSCs). A number of studies have found that increased migratory capacity and invasiveness of glioma is caused by mesenchymal transition.^{4–6} In malignant gliomas, GSCs and the mesenchymal transition contribute to tumor progression.^{7–11} Characterizing the common factors that modulate

glioma stemness and the mesenchymal transition simultaneously may aid in the development of new diagnostic, prognostic, and therapeutic approaches.

Circular RNAs (circRNAs), a new class of non-coding RNA (ncRNA) lacking a 5' cap and 3' polyadenylated (poly[A]) tail,^{12,13} present with a closed continuous loop structure. circRNAs have been reported to function via a variety of ways, including as microRNA (miRNA) sponges, RNA-binding proteins (RBPs), or serving as a transcriptional regulator.^{14–18} Recently, a series of studies demonstrated that circRNAs were associated with many cancer types via sponging miRNAs and by inhibiting miRNA activity in breast cancer,¹⁹ bladder cancer,²⁰ lung cancer,²¹ and glioma.^{22,23}

Eph receptor B2 (EphB2) is a member of the Eph receptor tyrosine kinase transmembrane glycoprotein family, exerting vital functions during development and cellular homeostasis, such as migration, cell adhesion, and axon guidance.^{24–26} Recent studies have also confirmed that EphB2 is associated with the migration of glioma cells and GSCs.^{27,28} However, whether EphB2 renders glioma cells' abilities of robust self-renewal and aggressive invasion remains unknown.

Wang et al.²⁹ sequenced circRNAs in three paired GBM tissues (GBM versus adjacent normal). Based on their study, we screened several circRNAs upregulated in glioma tissues, alongside normal tissues. Considering the size and the expression profiled in glioma cell lines and normal human astrocytes (NHAs) of these selected circRNAs, we selected circular *Maternal Embryonic Leucine Zipper Kinase* (circMELK, cMELK), which is derived from the MELK gene, for further study. Here, we demonstrated that circMELK is upregulated in glioma tissues and cell lines. Importantly, we found that circMELK could act

Received 15 November 2020; accepted 5 May 2021;
<https://doi.org/10.1016/j.omtn.2021.05.002>.

⁵These authors contributed equally

Correspondence: Ning Liu, Department of Neurosurgery, The First Affiliated Hospital of Nanjing Medical University, Nanjing 210029, Jiangsu Province, China.
E-mail: liuning0853@126.com

Correspondence: Haifeng Zhu, Department of Neurosurgery, Funing Hospital, Funing 224400, Jiangsu Province, China.

E-mail: gaobao720@163.com



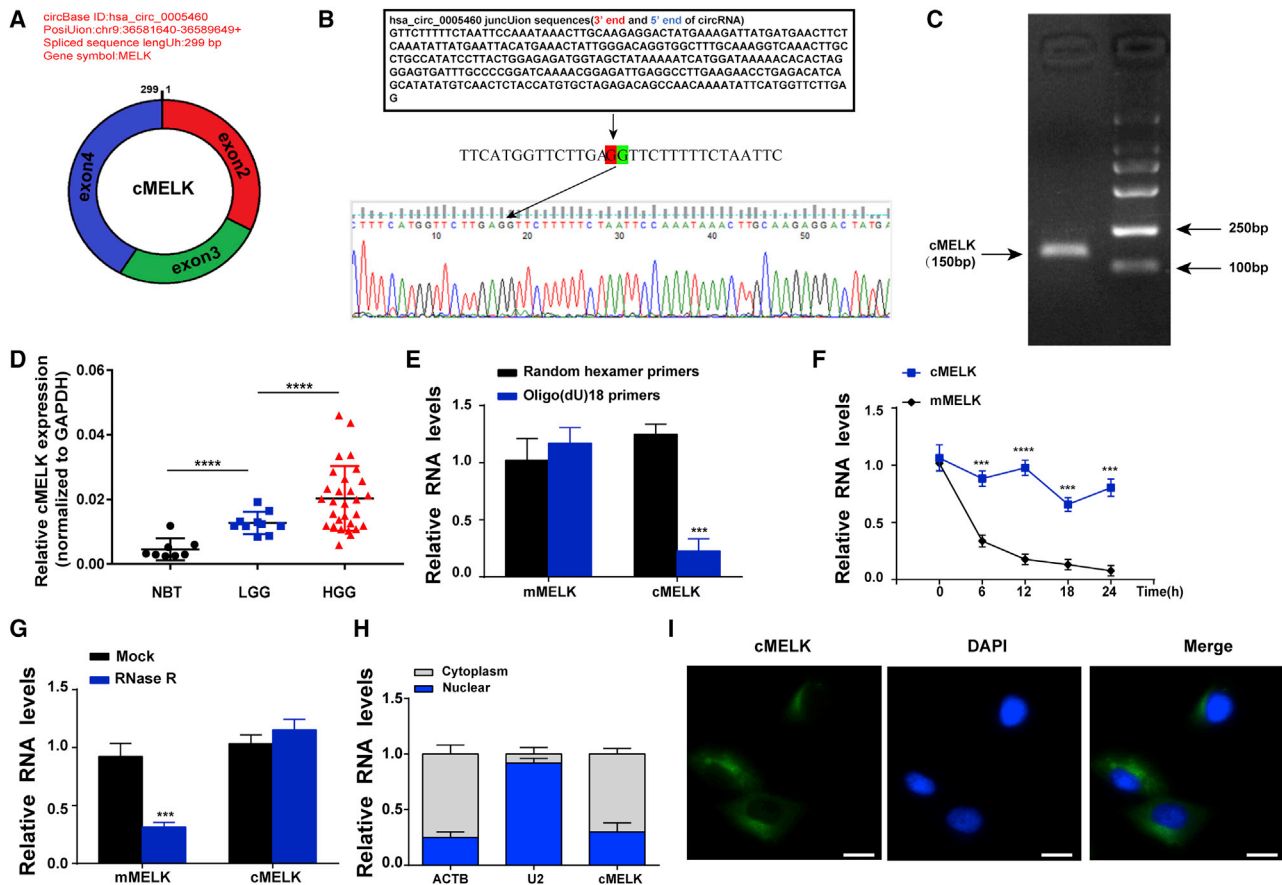


Figure 1. Characterization and expression of cMELK in glioma

(A) The exonic information of cMELK (circBase ID: has_circ_0005460) is illustrated as indicated. (B) Schematic representation of cMELK formation. The splice junction sequence was validated by Sanger sequencing and (C) agarose gel electrophoresis (right panel). The cDNA length of cMELK is 150 bp. (D) The levels of cMELK in 8 normal brain tissues (NBTs), 10 low grade glioma (LGG), and 30 high grade glioma (HGG) tissues were examined by qRT-PCR. (E) Random hexamer or oligo (dT) 18 primers were utilized for reverse transcription assays. The relative RNA levels were examined by qRT-PCR and normalized to those generated using random hexamer primers. (F) The relative RNA levels were examined by qRT-PCR after treatment with actinomycin D at the indicated time points in U87 cells. (G) The relative RNA levels were examined by qRT-PCR after treatment with RNase R or mock in total RNAs derived from U87 cells. (H) The cellular distribution of cMELK was analyzed by cellular RNA fractionation assays. ACTB and U2 were used as cytoplasmic and nuclear positive controls, respectively. (I) The cellular distribution of cMELK was analyzed by fluorescence *in situ* hybridization (FISH). Green indicates cMELK. Nuclei were stained with 4',6'-diamidino-2-phenylindole (DAPI). Scale bar, 50 μ m. All data are presented as the means \pm SD. Student's *t* test was used (***p* < 0.001, *****p* < 0.0001).

by sponging miR-593 to upregulate EphB2 expression and consequently enhance the proliferation, migration, invasion, and self-renewal of GBM cells. Understanding the molecular mechanism of the circMELK/miR-593/EphB2 axis in glioma development may help found a unique RNA-based therapy for GBM management.

RESULTS

Characterization and expression of cMELK in glioma

Bioinformatics analysis showed that cMELK originates from the second through fourth exons of the MELK gene, a novel circRNA that has not been studied in glioma previously. The mature length after splicing of cMELK is 299 bp (Figure 1A).³⁰ Specific PCR primers are first designed for cMELK and then validated by Sanger sequencing and agarose gel electrophoresis (Figures 1B and 1C), to measure its

expression level in glioma tissues. cMELK expression was significantly upregulated in 30 high-grade glioma (HGG) tissues compared with 10 low-grade glioma (LGG) tissues and 8 normal brain tissues (NBTs) according to qRT-PCR (Figure 1D).

The circRNA characteristics of cMELK were confirmed by a series of experiments. First, cMELK and mock expression vectors were constructed, and the efficiency of the cMELK overexpression vector was verified by qRT-PCR in GBM cells (U87; Figures S1A and S1B). Next, we applied random hexamer or oligo (dT)₁₈ primers in reverse transcription experiments using total RNA from U87 cells. When oligo (dT)₁₈ primers were applied, the relative expression of cMELK was remarkably reduced compared to random hexamer primer. On the contrary, the expression of the mature MELK

messenger RNA (mMELK mRNA) remained unchanged, which demonstrated that cMELK has no poly(A) tail (Figure 1E). Then, the half-life of cMELK and mMELK in pGBM-1 cells was measured after applying the transcription inhibitor actinomycin D, finding that cMELK was more stable than mMELK (Figure 1F). Considering the resistance of circRNAs to RNase R and higher stability than linear RNA,³¹ RNase R was applied to digest total RNAs. The results indicated that cMELK was much more resistant to RNase R than linear MELK mRNA (Figure 1G). Moreover, we found that cMELK was mainly localized in the cytoplasm of GBM cells (U87) through cellular RNA fractionation (Figure 1H) and fluorescence *in situ* hybridization (FISH; Figure 1I). In conclusion, cMELK is proved to be a stable and circular transcript.

cMELK enhanced GBM mesenchymal transition and GSC maintenance *in vitro*

The expression of cMELK was detected in NHAs, GBM cell lines (U251, LN229, U118, U87, and T98G), and one primary cell line (pGBM-1) derived from an adult primary GBM sample. cMELK was highly expressed in U87 and pGBM-1 cells (Figure 2A), and therefore U87 and pGBM-1 cells were selected for silencing of cMELK experiments. First, loss-of-function studies were performed using lentiviral transduction of independent small hairpin RNAs (shRNAs) targeting cMELK (designated as shRNA-1, shRNA-2, and shRNA-3; Figure 2B). The efficiency of cMELK knockdown was confirmed by real-time PCR, and shRNA-2 (shcMELK) was chosen for further study (Figure 2C). Silencing cMELK remarkably downregulated the mesenchymal markers and transcription factors N-cadherin, Vimentin, Snail, Slug, MMP2, and MMP9 (Figure 2D). Further, immunofluorescence was conducted to analyze the expression of N-cadherin, and Vimentin in glioma cells, and indicated the strong correlation of the decrease of N-cadherin and Vimentin and the decline of cMELK in the transduced cells (Figure 2E). Transwell migration and three-dimensional spheroid assays demonstrated that the capacity of migration and invasion in both indicated cells were decreased (pGBM-1-shcMELK and pGBM-1/GFP tumorspheres-shcMELK; Figures 2F and 2G) and phenocopied in U87-shcMELK and U87/GFP tumorspheres-shcMELK cells (Figures S2A and S2B).

cMELK impacted the sphere-forming capacity, GSC growth, and cell viability of GSCs derived from U87 and pGBM-1 cells, and expression of GSC markers was further investigated by confocal microscopy. The co-localization of GSC markers (Nestin and Sox2) and the sphere size, often considered a surrogate of proliferation, were smaller in GSCs-shcMELK cells than in GSCs-transduced non-targeting control shRNAs (shCONT) cells (Figure 2H). Simultaneously, a clonogenic assay revealed that the percentage of positive wells in GSCs-shcMELK was lower than in GSCs-shCONT (Figure 2I). Subsequently, pluripotency factors including Nestin, Sox2, Nanog, and Oct4 were evaluated via western blot assays (Figure S2C). The knockdown of cMELK decreased GSCs growth and cell viability (Figures 2J and 2K), supporting that cMELK may play a key role in GBM cell mesenchymal transition and GSC maintenance.

Knockdown of cMELK inhibits GBM growth *in vivo*

To further examine the effect of cMELK on glioma cells *in vivo*, we co-transfected pGBM-1 cells with a lentivirus expressing luciferase and shCONT or shcMELK. Nude mice were intracranially xenotransplanted with the treated pGBM-1 cells and a live animal bioluminescence imaging system was used weekly to monitor tumor growth after implantation (Figure 3A). The growth of intracranial tumors was impeded significantly by silencing of cMELK, as determined on days 14, 21, and 28 (Figure 3B). Kaplan-Meier survival curves showed that the survival of nude mice injected with shcMELK cells was remarkably longer (Figure 3C). Furthermore, immunohistochemical (IHC) experiments suggested that the tumor specimens derived from shcMELK pGBM-1 cells displayed lower expression of Vimentin, MMP2, and SOX2 (Figure 3D), consistent with the results obtained from the *in vitro* studies. These findings strongly demonstrated that cMELK plays an oncogenic role to the tumorigenesis of GBM *in vivo*.

cMELK acts as a sponge for miR-593

The previous results suggested that cMELK was predominately distributed in the cytoplasm, indicating that cMELK mainly acts as a sponge of miRNAs. To explore whether cMELK functions as a miRNA sponge in GBM specifically, we conducted RNA immunoprecipitation (RIP) assays with an AGO2 antibody. Results of qPCR and agarose gel electrophoresis showed that the enrichment of cMELK was remarkably increased by the AGO2 antibody and decreased by the immunoglobulin G (IgG) antibody (Figures 4A and 4B). These results demonstrated that cMELK binds AGO2 and miRNAs. circRNA interactome database was used to investigate potential miRNA targets (Figure 4C). circRNA *in vivo* precipitation (circRIP) assay was subsequently performed with a cMELK-specific probe. cMELK and miR-593 were significantly enriched by the cMELK-specific probe compared with the other miRNAs (Figure 4D), indicating miR-593 as a potential target of cMELK in GBM cells.

To further confirm the miRNA target, we performed dual-luciferase reporter assays. The data revealed that the transfection with an miR-593 mimic observably attenuated the luciferase activity of wild-type (WT) cMELK vector compared with the mutant cMELK vector (Figures 4E and 4F). Moreover, knockdown of cMELK in U87 and pGBM-1 cells significantly increased miR-593 expression (Figure 4G). Further, immunofluorescence analysis suggested that cMELK and miR-593 were co-localized in the cytoplasm of U87 and pGBM-1 cells (Figure 4H). The expression of miR-593 in NBT and gliomas was also investigated by qRT-PCR. The expression level of miR-593 was remarkably lower in glioma tissues compared with NBTs (Figure 4I). Spearman's correlation analysis further indicated that miR-593 expression in glioma samples was inversely correlated with the expression level of cMELK (Figure 4J). Together, these data suggest that cMELK can function as a sponge for miR-593 in GBM cells.

EphB2 is a direct target of miR-593

To examine the role and clinical significance of miRNA-593, we used Chinese Glioma Genome Atlas (CGGA) data to analyze the

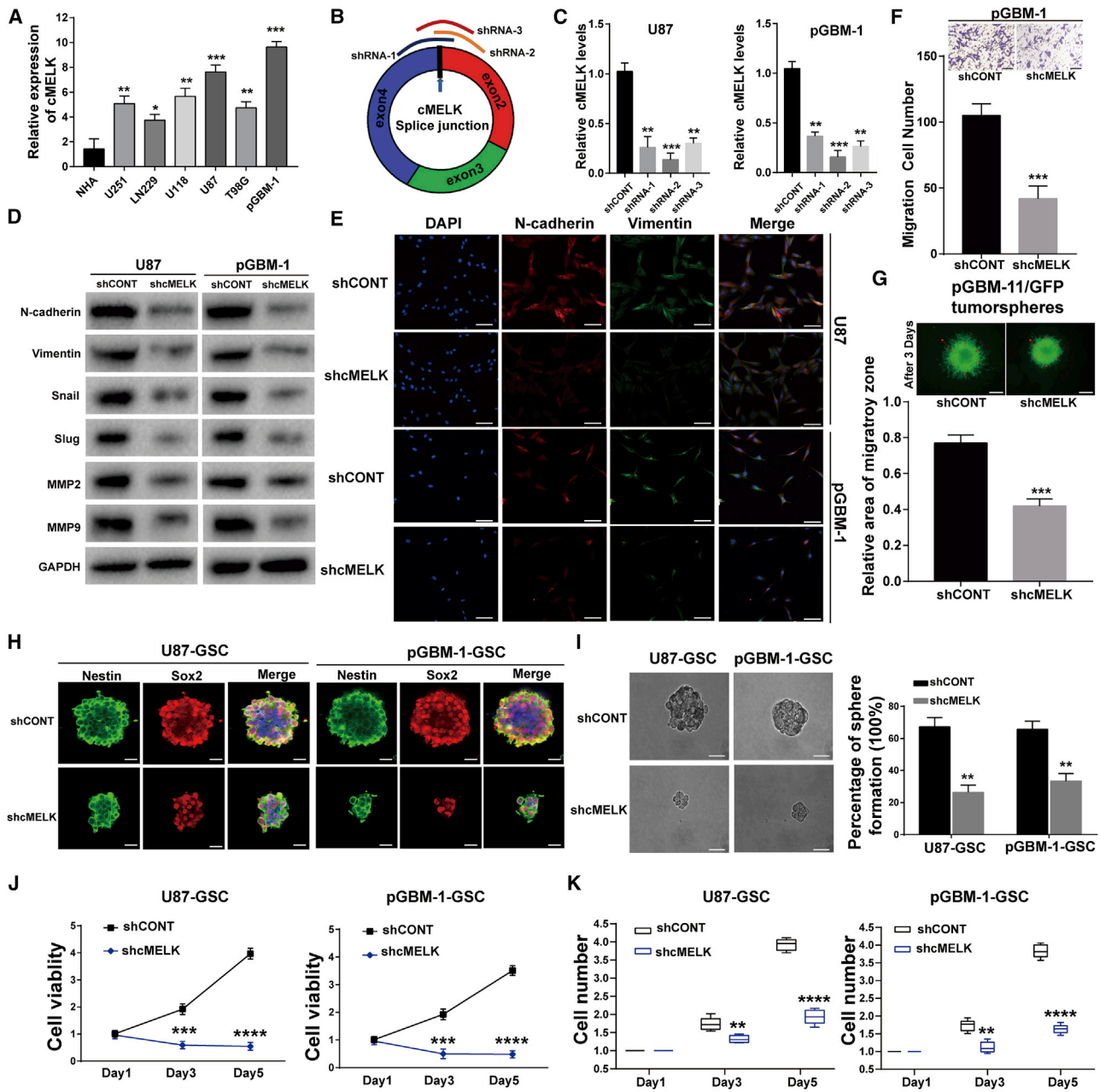


Figure 2. cMELK enhanced GBM mesenchymal transition and GSC maintenance *in vitro*

(A) The expression levels of cMELK in normal human astrocytes (NHAs) and GBM cells were analyzed by qRT-PCR. (B) Schematic representation of designed shRNAs (shRNA-1, shRNA-2, and shRNA-3) for cMELK at splice junctions. (C) qRT-PCR detected the expression of cMELK in U87 and pGBM-1 cells transduced with either a non-targeting control shRNA (shRNA) or shRNA-2 targeting cMELK (shcMELK). (D) Western blot analysis of N-cadherin, Vimentin, Snail, Slug, MMP2, and MMP9 in U87 and pGBM-1 cells after transfection, GAPDH served as the loading control. (E) Immunofluorescence staining of N-cadherin (red), and Vimentin (green) in treated U87 and pGBM-1 cells. Scale bar, 100 μ m. (F) The transfected pGBM-1 cells migration was examined by Matrigel migration assay. Scale bar, 100 μ m. (G) Invasion of treated pGBM-1/GFP tumor-spheres was monitored by three-dimensional spheroid assays. Representative images and quantification at day 3 post plating. Scale bar, 50 μ m. (H) Colocalization of Nestin (green) and Sox2 (red) in treated U87-GSCs and pGBM-1-GSCs showed by confocal images. Nuclei were counterstained with DAPI (blue). Scale bar, 50 μ m. (I) Clonogenic assay was used to measure the stemness of GSCs after transfection. Representative photomicrographs of new clonal sphere (left) and statistical analysis of the percentage of positive wells (right). Scale bar, 50 μ m. (J) The cellular effects were transduced U87-GSCs and pGBM-1-GSCs were assessed by CellTiter-Glo assay. (K) The cellular effects were transduced U87-GSCs and pGBM-1-GSCs were assessed by direct cell count. Data are presented as the means of triplicate experiments (* $p < 0.05$, ** $p < 0.01$, *** $p < 0.001$, **** $p < 0.0001$).

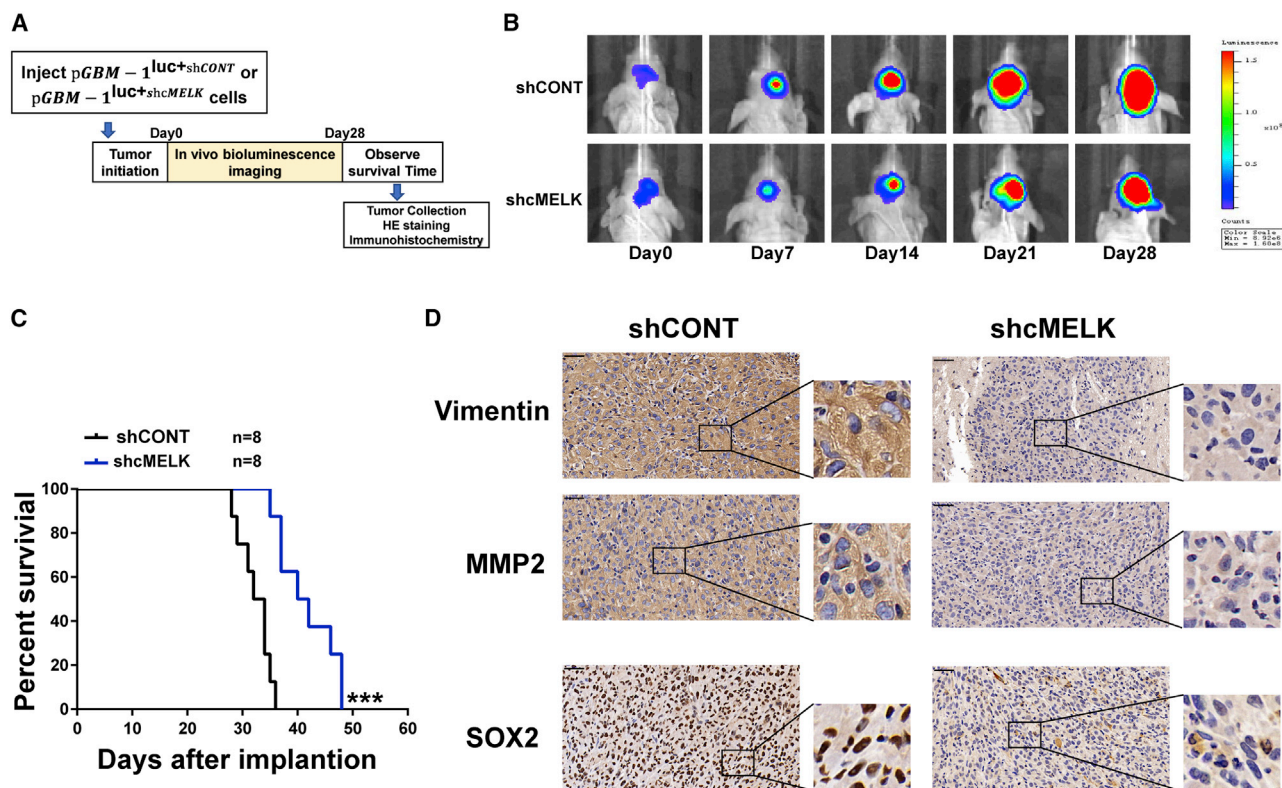


Figure 3. Knockdown of cMELK inhibits GBM growth *in vivo*

(A) The panel shows a schematic presentation of *in vivo* experiment. (B) After the beginning of treatment, nude mice were monitored by luciferase live imaging system weekly. (C) Kaplan-Meier analysis of overall survival of the shCONT group and the shcMELK group. (D) Immunohistochemistry on xenografted tumors from both the shCONT group and shcMELK group. Scale bar, 50 μ m. The data are presented as the means \pm SD. Student's t test was used (** $p < 0.001$).

expression of miR-593 and the associated clinical prognosis in glioma. The expression of miR-593 in WHO II glioma was significantly higher than in WHO III and WHO IV gliomas (Figure 5A), and increased miR-593 expression was associated with a longer survival period especially in the CGGA database (Figure 5B). The bioinformatics tools TargetScan, miRDB, DIANAmt, miRanda, and RNAhybrid were employed to identify potential targets of miR-593, identifying EphB2 as a potential target gene of miR-593 (Figure 5C). In the CGGA database, EphB2 mRNA was found to be significantly higher in WHO IV glioma, compared with WHO II and WHO III gliomas (Figure 5D), and increased EphB2 expression was associated with a shorter survival period (Figure 5E). Meanwhile, in The Cancer Genome Atlas (TCGA) database, EphB2 mRNA levels were found to be significantly upregulated in GBM specimens as compared with NBTs (Figure S3). Considering that miRNAs perform key functions via binding to the 3' untranslated region (3' UTR) of target mRNA to downregulate gene expression, we prognosticated that EphB2 could be the direct target of miR-593. The miRNA-related algorithms were executed to identify the miR-593-binding sites in the 3' UTR of EphB2 mRNA (Figure 5F). Next, luciferase reporter assays were performed to confirm that miR-593 could directly bind to the 3' UTR of EphB2. U87 and pGBM-1 cells were co-transfected with vectors

harboring WT or mutant EphB2 3' UTRs and miR-593 mimic (Figure 5G). WT and mutated binding site 2 of the EphB2 3' UTR both led to significantly decreased luciferase activity in U87 and pGBM-1 cells co-transfected with miR-593 mimics. On the other hand, mutation of binding site 1 nearly rescued the decreased activity (Figure 5H). Collectively, data indicated that miR-593 directly regulates EphB2 expression through its binding to site 1 (nt134-140) in the 3' UTR of EphB2.

cMELK promotes mesenchymal transition and GSC maintenance of GBM cells through the miR-593/EphB2 pathway

Next, we explored the interaction between cMELK and miR-593 and its role in regulating EphB2 expression, malignant behavior of GBM cells, and GSC maintenance. We found that cMELK knockdown significantly decreased EphB2 mRNA and protein levels in U87 and pGBM-1 cells, an action that could be rescued by inhibiting miR-593 (Figures 6A and 6B). Functionally, Transwell migration and three-dimensional spheroid assays showed that the knockdown of cMELK inhibited the migration and invasion of GBM cells and that miR-593 inhibitors could also reverse the inhibitory effect (Figures 6C-6F). Moreover, the inhibitory effects of GSC maintenance by silencing cMELK were blocked via inhibition of miR-593

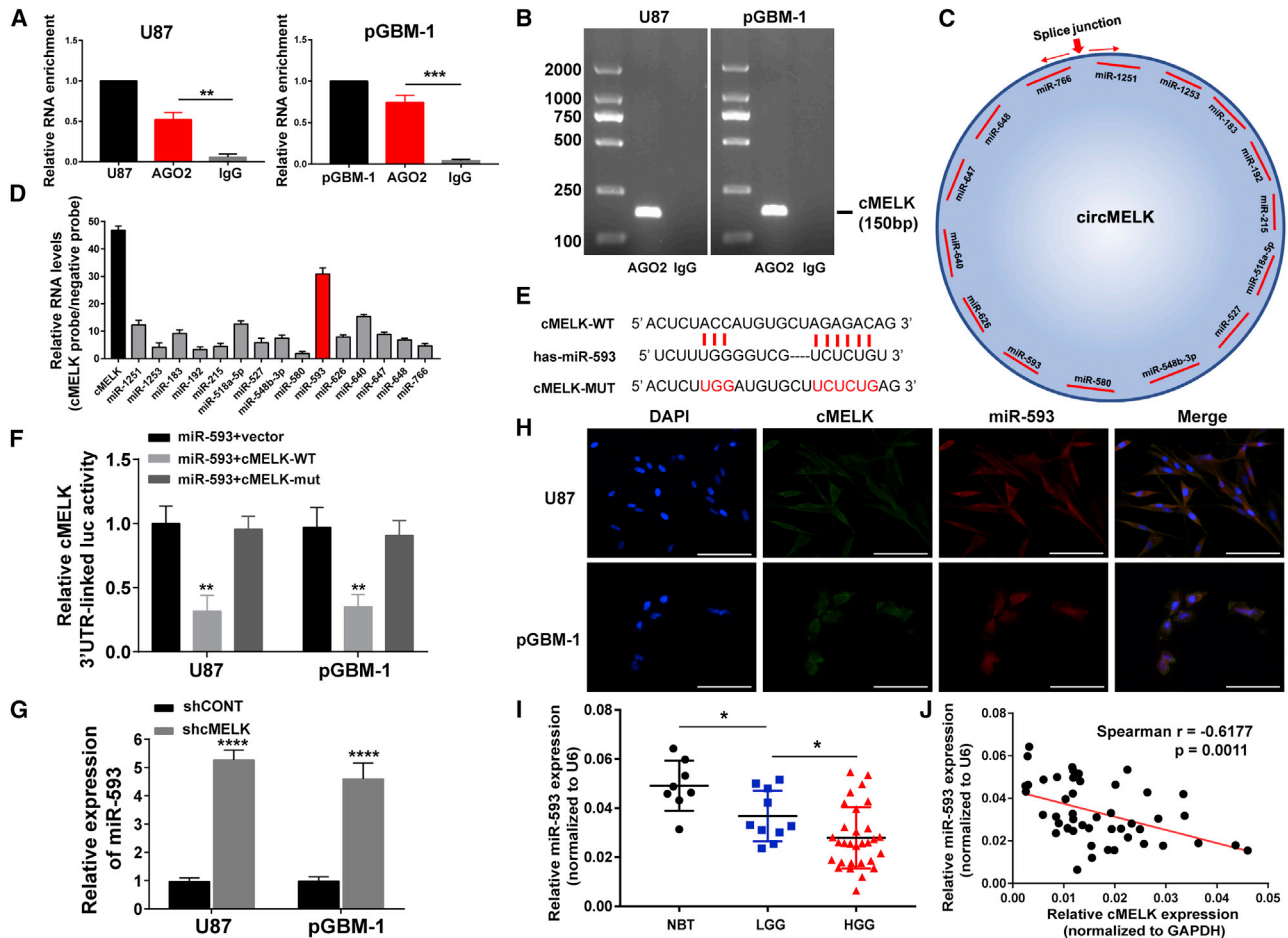


Figure 4. cMELK acts as a sponge for miR-593

(A) The binding of cMELK to the AGO2 protein was analyzed by RNA immunoprecipitation (RIP) and qRT-PCR assays. (B) The binding of cMELK to the AGO2 protein was detected by agarose gel electrophoresis assays. The cDNA length of cMELK is 150 bp. (C) The binding sites of miRNAs and cMELK were predicted by circular RNA (circRNA) interactome. (D) circRNA *in vivo* precipitation (circRIP) assays were performed using cMELK-overexpressing U87 cells with a cMELK-specific probe and NC probe. qRT-PCR was performed to analyze potential miRNAs associated with cMELK. The enrichment of cMELK and potential miRNAs were normalized to that of the control probe. (E) The putative binding sites of miR-593 between the wild-type (WT) and mutated-type (MUT) sequences of cMELK. (F) The association of cMELK and miR-593 was validated by dual-luciferase reporter assays. (G) The expression of miR-593 was validated by qRT-PCR in treated U87 and pGBM-1 cells. (H) Colocalization of cMELK and miR-593 in transfected U87 and pGBM-1 cells was measured by FISH. Scale bar, 100 μ m. (I) The expression of miR-593 in 8 NBT, 10 low grade gliomas (LGG), and 30 high grade gliomas (HGG) was examined by qRT-PCR. (J) Pearson's correlation test was used to evaluate the correlation between the expression of cMELK and miR-593 ($r^2 = -0.6177$, $p = 0.0011$). Data are presented as the means of triplicate experiments. Student's t test was used (* $p < 0.05$, ** $p < 0.01$, *** $p < 0.001$, **** $p < 0.0001$).

(Figure 6G–6J). Taken together, these results demonstrated that cMELK plays a key role in promoting the mesenchymal transition and GSC maintenance of GBM cells via the miR-593/EphB2 pathway (Figure 7).

DISCUSSION

Growing evidence has demonstrated that the poor prognosis of GBM patients may be due to its rapid proliferation and infiltrative growth, resulting in obstacles for resection and recurrence.³² The cellular hierarchy of GBM has been consistently demonstrated, reflected in the contribution of GSCs to tumor growth, invasion into normal brain tissues, and recurrence of glioma.^{33–35} The mesenchymal transition

not only facilitates the invasion of GBM but also the progression of GSCs.^{36,37} Therefore, there remains a pressing need to decipher the underlying mechanisms of this transition, especially in the treatment of gliomas.

Emerging evidence has shown that circRNAs play a role in regulating the progression of glioma.^{38–40} In this study, we focused on cMELK, a functioning oncogene, and investigated its biological role in glioblastoma tumorigenesis. Considering the relation of mesenchymal transition and glioma stemness, we hypothesized that cMELK not only regulated the mesenchymal transition program, but also promoted glioma stem cell-like phenotypes. We found that the expression of

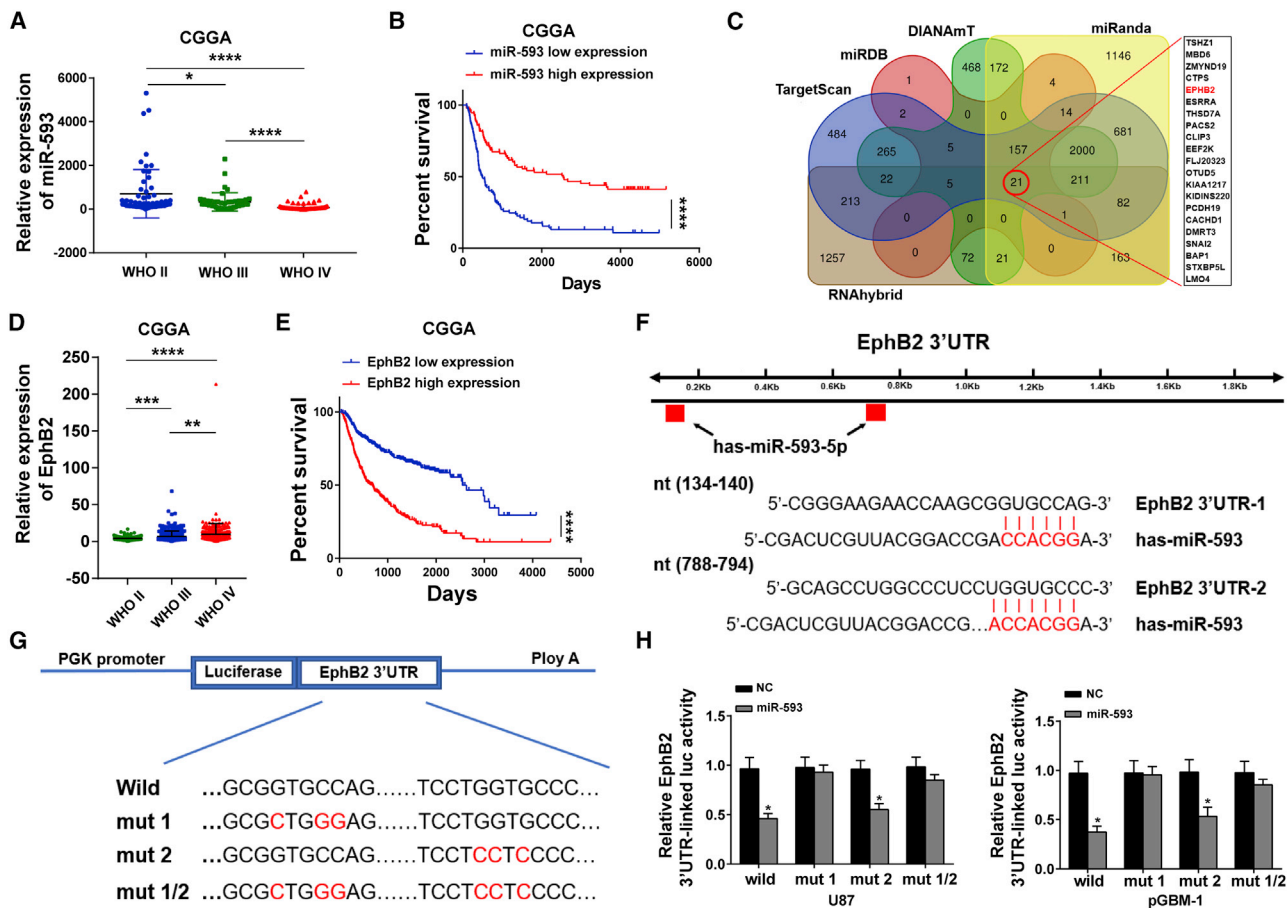


Figure 5. EphB2 is a direct target of miR-593

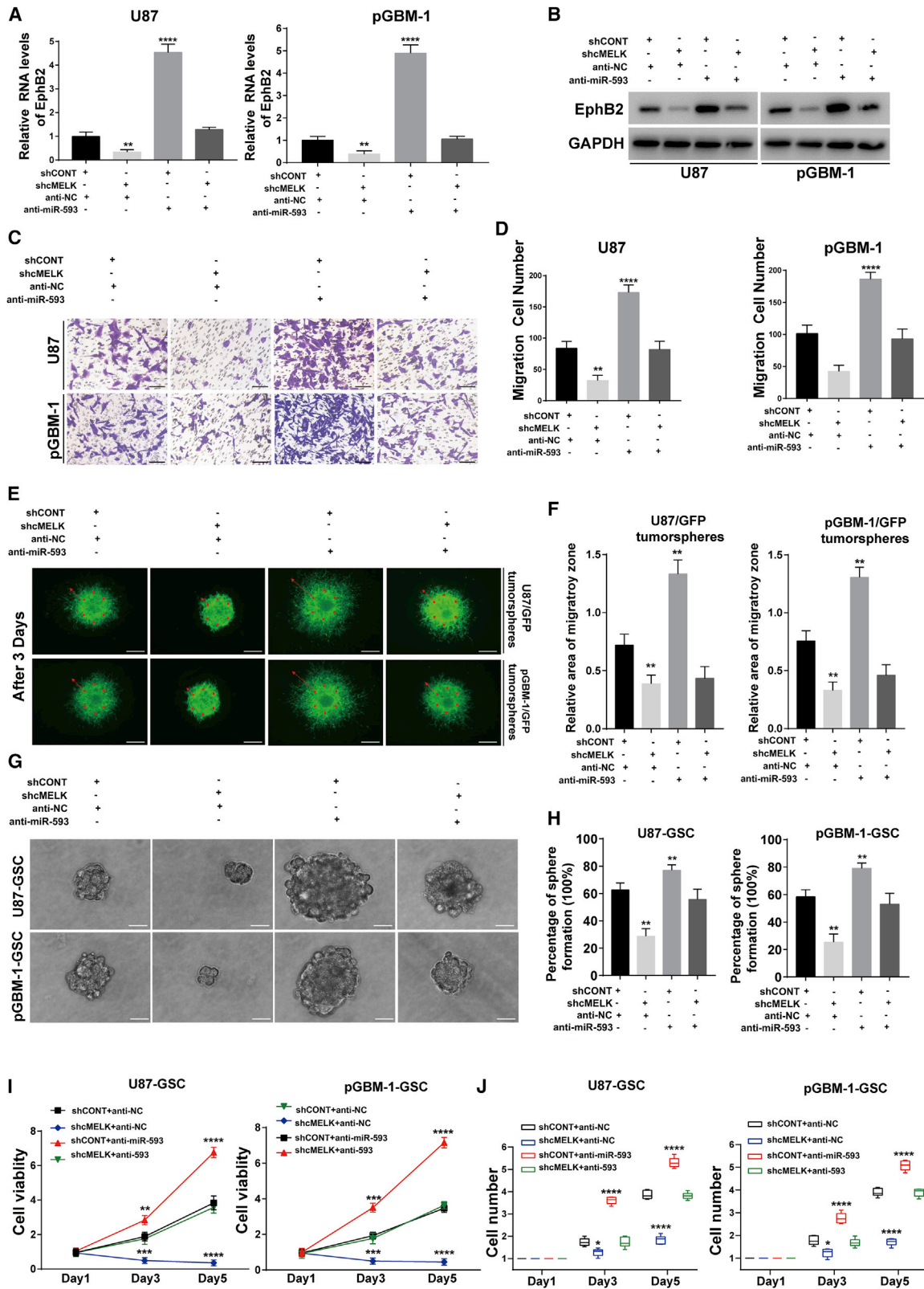
(A) The expression of miR-593 in The Chinese Glioma Genome Atlas (CGGA) database of human glioma patients. (B) Kaplan-Meier survival curve was used to estimate the survival outcomes of patients divided into two groups with miR-593 low/high level using CGGA database. (C) miR-593 computationally predicted to target 21 candidates by five different prediction algorithms (DIANA-T, TargetScan, miRDB, miRanda, and RNAhybrid) were displayed by Venn diagram. (D) The expression of EphB2 in CGGA database of human glioma patients. (E) Kaplan-Meier survival curve was used to estimate the survival outcomes of patients divided into two groups with EphB2 low/high level using CGGA database. (F) The predicted miR-593-binding sequence in the *EphB2* 3' UTR. (G) WT and mutant *EphB2* 3' UTR reporter constructs. (H) Dual-luciferase reporter assay was performed on U87 (left) and pGBM-1 (right) cells, which were co-transfected with the indicated WT or mutant 3' UTR construct and the miR-593 mimics. Data are presented as the means of triplicate experiments. Student's t test was used (*p < 0.05, **p < 0.01, ***p < 0.001, ****p < 0.0001).

cMELK was significantly increased in 40 gliomas compared with 8 NBT samples. cMELK was stably expressed and that knockdown suppressed the migration, invasion, and the GSC maintenance of GBM *in vitro*, as well as tumor growth *in vivo*.

Recently, a number of studies reported that circRNA acts mainly as a miRNA sponge to regulate gene expression, serving as a cancer promoter or tumor suppressor.^{21,41} Considering that cMELK was primarily localized in the cytoplasm, we hypothesized that cMELK may act by sponging miRNA. To verify miRNAs targeted by cMELK, we used bioinformatic tools, circRNA *in vivo* precipitation, dual-luciferase reporter, and co-localization assays to verify the sponging capacity of cMELK on miR-593. Additionally, we found that EphB2, a regulator of the migration, invasion, and stem cell-like phenotype,⁴²⁻⁴⁴ was indeed a target gene of the circMELK/miR-593 axis. Luciferase

reporter assays confirmed that miR-593 could specifically bind to the 3' UTR region (site 1) of the EphB2 transcript. Noticeably, miR-451 and miR-185 function as fibrosis suppressors and act synergistically to inhibit liver fibrosis via co-targeting *EphB2*,⁴⁵ and miR-204 could inhibit the proliferation and invasion of human cervical cancer via targeting *EphB2*.⁴⁶ Hence, it is important in our further studies to find whether there exist some other miRNAs that also bind to site 1 or nearby loci of *EphB2* and function synergistically with miR-593 in glioma. Second, cMELK knockdown significantly decreased *EphB2* mRNA and protein levels in U87 and pGBM-1 cells, which could be rescued by inhibiting miR-593. These data uncovered the oncogenic function of circMELK in glioma progression.

In conclusion, our current data demonstrated that the circRNA cMELK was upregulated in glioma tissues compared with normal



(legend on next page)

brain tissues. Functionally, cMELK promoted glioma cell migration, invasion, and GSC maintenance *in vitro* and tumor growth *in vivo*. Mechanistically, cMELK increased EphB2 expression through sponging miR-593. Collectively, our study illuminated the key role of cMELK/miR-593/EphB2 axis in the GBM development. This novel finding not only improves our knowledge of the molecular mechanisms underlying glioma tumorigenesis, but also points to a promising therapeutic strategy against glioma.

MATERIALS AND METHODS

Human tissue samples

40 human glioma samples were obtained from surgical resection specimens of glioma patients at the First Affiliated Hospital of Nanjing Medical University (Nanjing, China). In addition, eight NBT samples were collected as negative controls from patients who underwent decompressive craniotomy for severe traumatic brain injury. The samples were quickly frozen in liquid nitrogen after surgery immediately. Both glioma and NBT samples were confirmed histologically. Our study protocol was approved by the Research Ethics Committee of Nanjing Medical University (Nanjing, Jiangsu, China).

Cell culture, transfection, and establishment of stably virus-transduced cell lines

Five human glioblastoma cell lines (U251, LN229, U118, U87, and T98G) were purchased from the Chinese Cell Repository (Shanghai, China). Primary GBM cells (pGBM-1) that derived from a GBM surgical specimen were maintained in DMEM supplemented with 10% FBS. NHAs were obtained from ScienCell Research Laboratories (Carlsbad, CA, USA). Oligonucleotide sequences of cMELK were as follows: #shRNA-1: 5'-CATGGTTCTTGAGGTTCTTTT-3', #shRNA-2: 5'-GGTTCTTGAGGTTCTTTTCT-3', and #shRNA-3: 5'-CTTGAGGTTCTTTTCTAATT-3'. For regulating cMELK the sequence was cloned into pcDNA3.1 vector (RioBio, Guangzhou, China), namely pcDNA-cMELK, with pcDNA-NC as control. miR-593 inhibitors (anti-miR-593), miR-593 mimics (miR-593), and their paired control (anti-NC and miR-NC) were obtained from Genechem (Shanghai, China). Lentivirus vectors with shRNAs or shCONT and anti-miR-593 or anti-NC were purchased from Genechem (Shanghai, China). Stable U87 and pGBM-1 cell lines were established by lentiviral infection and puromycin selection following the manufacturer's instructions.

qRT-PCR

Total RNA was extracted from harvested cells or human tissues with TRIzol reagent according to the manufacturer's instructions (Life

Technologies, Carlsbad, CA, USA). RNase R treatment was carried out for 30 min at 37°C using 3 U/mg of RNase R (Epicenter Technologies, RNR07250). qRT-PCR was implemented utilizing QuantiTect SYBR Green PCR Kit (QIAGEN) or all-in-one miRNA qRT-PCR Detection Kit (GeneCopoeia, Guangzhou, China). The relative expression of circMELK, MELK mRNA, miR-593, and EphB2 was calculated through the $2^{-\Delta\Delta Ct}$ method, with glyceraldehyde-3-phosphate dehydrogenase (GAPDH; for circMELK, MELK mRNA, and EphB2) or U6 (for miR-593) as internal reference. Primers for qRT-PCR were purchased from Genepharma (Shanghai, China), and sequences were as follows: circMELK, forward: 5'-TTGAGG CCTTGAAGAACCTG-3', reverse: 5'-CCACCTGTCCCAATAGTT TCA-3'; MELK mRNA, forward: 5'-ACTGCCCTGGAGGAGAGC TG-3', reverse: 5'-AGCCCTGGCTGTGCACATAA-3'; GAPDH, forward: 5'-ACCCACTCCTCCACCTTTGA-3', reverse: 5'-CTGTTGC TGTAGCCAAATTCGT-3'; miR-593, forward: 5'-GTGGTCATGTA GCGTCGATTT-3', reverse: 5'-ATTTGCATGCTACGCTATTAC-3'; and U6, forward: 5'-GCTTCGGCAGCACATATACTAAAAT-3', reverse: 5'-CGCTTCAGAATTTGCGTGTTCAT-3'. Products were separated on a 2% agarose gel and visualized with GelRed. All experiments were performed in triplicate and repeated three times.

Western blot analysis

Cells were fully mixed with radioimmunoprecipitation assay (RIPA) lysis buffer (KeyGEN, Jiangsu, China) to extract proteins. After centrifuging at 12,000 rpm speed, liquid supernatant was collected and then separated by equal amounts of SDS-PAGE, followed by electro-transfer onto polyvinylidene difluoride membranes (Thermo Fisher Scientific, MA, USA). Subsequently, membranes were blocked with 5% nonfat milk for 2 h. Primary antibody was diluted to 1:1,000 and then incubated with membrane at room temperature. Secondary antibody was used to combine primary antibody for 2 h. Finally, membranes were developed using an enhanced chemiluminescence detection system (GE Healthcare, Chicago, IL, USA). Immunoblot analysis used the following primary antibodies purchased from Cell Signaling Technology (Danvers, MA, USA): anti-EphB2 (#83029), N-cadherin (#14215), Vimentin (#5741), MMP2 (#40994), MMP2 (#13667), Snail (#3879), Slug (#9585), Sox2 (#3579), Nestin (#33475), Nanog (#8822), Oct-4 (#2750), and GAPDH (#5174).

Glioma stem cell culture, spheroid formation assay, and clonogenic assays

To generate GSCs derived from adherent U87 and pGBM-1 cells, we used DMEM/F12 (GIBCO), supplemented with B27(1/50, Invitrogen), N2(1/100, Invitrogen), 10 ng/mL recombinant human

Figure 6. cMELK promotes mesenchymal transition and GSC maintenance of GBM cells through the miR-593/EphB2 pathway

(A) qRT-PCR assays detected the expression levels of *EphB2* in the U87 and pGBM-1 cells upon cMELK knockdown alone or silencing miR-593 alone or in combination. (B) Western blot analysis of EphB2 in the indicated cells, GAPDH served as the loading control. (C and D) Representative images and quantification of Matrigel invasion for transfected U87 and pGBM-1 cells. Scale bar, 100 μ m. (E and F) Representative images and quantification of three-dimensional spheroid assays for transfected U87/GFP tumor-spheres and pGBM-1/GFP tumor-spheres. Scale bar, 50 μ m. (G) Representative photomicrographs of new clonal sphere after transduced. (H) The statistical analysis of the percentage of positive wells of clonogenic assay were measured the stemness of GSCs after transduced. Scale bar, 50 μ m. (I and J) The cellular effects of transduced U87-GSCs and pGBM-1-GSCs were assessed by CellTiter-Glo assay and direct cell count. Data are presented as the means of triplicate experiments. Student's t test was used (**p < 0.01, ***p < 0.001, ****p < 0.0001).

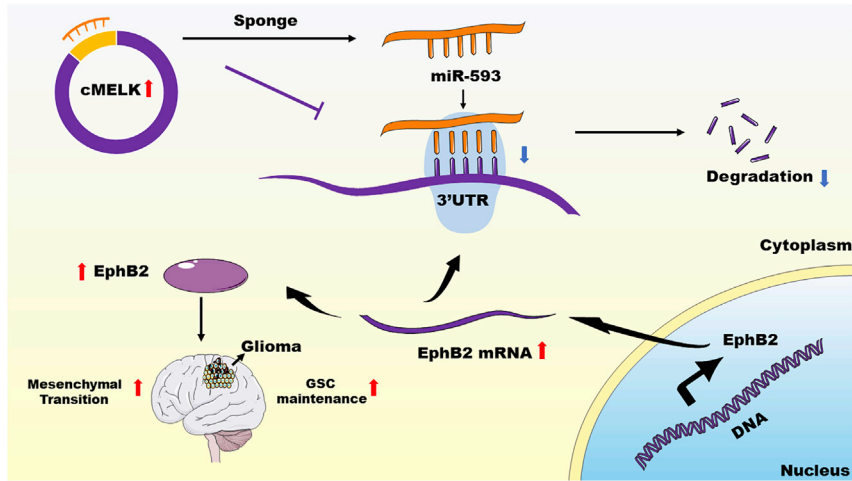


Figure 7. Schematic diagram of the cMELK-mediated pathway in GBM cells

cMELK upregulation increased the adsorption of miR-593, which increases the degradation of *EphB2* and thus promotes GBM mesenchymal transition and GSC maintenance.

RNA FISH

Cy3-labeled circMELK and Dig-labeled miR-593 probes were synthesized by RiboBio (Guangzhou, China). The signals of the probes were detected by the FISH Kit (RiboBio, China) according to the manufacturer's instructions.

RIP assay

Magna RIP Kits (Millipore, USA) were purchased for RNA-binding protein immunoprecipitation assays, which was performed according to instruction. Cells were lysed in RIP lysis buffer, and cell lysate was later co-incubated with magnetic beads with AGO2 (Abcam ab32381) or IgG antibody together with rotation at 4°C overnight. qPCR was used to analyze cDNA, which was reverse transcribed by immunoprecipitated RNAs, and all data were normalized to the input control.

circRIP assay

Sample preparation

Cells were inoculated into a 10 cm culture dish and cultured for 48 h. Biotin-labeled probe and non-specific blank control probe were transfected at 200 nM, incubated at 37°C and 5% CO₂. 24 h after receiving the transfection probe, the cells were first fixed with 1% formaldehyde for 10 min and then treated with glycine solution for 5 min, washed three times by pre-cooling PBS, scratched with 1 mL lysate, and left standing for 10 min. The sample was then treated with ultrasound, centrifugating at 10,000 × *g* for 10 min. Finally, supernatant was transferred to a 2 mL centrifuge tube and 50 μL was taken and stored as input control.

Beads preparation and bond

First, streptavidin-labeled magnetic beads (Invitrogen) were washed twice with solution A (0.1M NaOH+ 0.05M NaCl) and then washed once with solution B (0.1M NaCl). The 100 μL magnetic beads suspension was coated with 10 μL BSA (10 mg/mL) and 10 μL tRNA (10 mg/mL), respectively, and mixed at room temperature fully reversed for 3 h. Finally, 500 μL lytic solution was used for washing twice, and 1 mL lytic solution was used for resuspending. The obtained supernatant was mixed with a probes-M280 streptavidin dynabeads mixture and then reversed for 1 h. The samples were washed twice with eluent A and B, resuspended with 200 μL lysate, and placed for 2 h for cross-linking.

RNA extraction

The sample was mixed with 300 μL Trizol, adding 100 μL chloroform after 5 min, vibrating for 30 s, then centrifuging at 10,000 × *g* for

epidermal growth factor (EGF, Invitrogen) and 10 ng/mL recombinant human basic fibroblast growth factor (FGF, Invitrogen), which was called sphere medium for short, to dedifferentiate the above cells. To further enrich the GSCs, we used TrypLETM Express (GIBCO) to dissociate GSC spheres when primary spheroids got a diameter >200 μm, then single cell population was resuspended in so-called sphere medium. After several times of sphere culture, we used these secondary cellular spheroids in the next experiments, which were considered as enriched in GSC. For testing the capacity of spheroid formation, sphere medium was added in 6-well plates together with moderate disaggregated spheres. A week later, we assessed the sphere formation capacity of GSC by counting the diameter of spheres bigger than 25 μm. For clonogenic assays, disaggregated spheres were seeded in 96-well plates at clonal density (1 cell per well). Every 5 days, sphere medium was replaced by fresh medium to supply nutrition. 15 days later, we counted the percentage of spheres formation.

Cell migration and invasion experiments

The ability of cell migration was measured using Transwell chambers (Corning, USA) with 8 μm pore filters according to the manufacturer's instructions. Cells were suspended in 200 μL serum-free medium (5 × 10⁴ cells per well). DMEM medium containing 20% FBS was added to the bottom of chambers. After incubation at 37°C for 24 h (migration assay), cells on the upper surface were removed with a cotton swab. Cells that migrated into the bottom of the membrane were fixed with 4% paraformaldehyde, stained with crystal violet solution, and then visualized under a microscope. The cell numbers were counted in five random fields of view.

To test cell invasion, we used a three-dimensional spheroid assay. Transfected cells were grown to 70% confluence and were then seeded in 96-well ultra-low adherence plates (#7007, Costar) at a density of 0.2 × 10⁵ cells/mL. 96 h later, these cells were induced to aggregate into a multicellular spheroid followed by supplement of matrigel at 48 h, and then fluorescence microscopy was used to analyze cell motion.

10 min. The centrifugal supernatant was transferred to the new EP (RNase – Free). 1 μ L DNAmate, 36 μ L 3 M NaCl, and 360 μ L isopropyl alcohol were used to precipitate RNA sample at 80°C for at least 1 h, and then samples were centrifuged at 12,000 $\times g$ for 30 min at 4°C. The supernatant was discarded, and the precipitation was washed with ethanol prepared with 500 μ L 70% RNASE-FREE water. The ethanol was carefully discarded. After drying at room temperature, the precipitate was resuspended with 50 μ L RNASE-FREE water. cMELK-specific probe sequence is as follows: 5'-GAATTAGAAAAAGAACC TCAAGAACCATGAATATTTTGTGGCTG-3'.

A dual-luciferase reporter assay

To construct luciferase reporters, we inserted the sequence of circMELK or EphB2 3' UTR containing the forecasted binding sites or mutant binding sites into pGL3 vector (Promega, Madison, WI, USA), namely circMELK-WT, circMELK-MUT, EphB2 3'UTR-WT, EphB2 3'UTR MUT1, and EphB2 3'UTR MUT2. U87 and pGBM-1 cells were co-transfected with luciferase reporter and miR-593 or miR-NC using Lipofectamine 3000. After 48 h, the luciferase activity was examined via a Dual Luciferase Reporter Assay Kit (Vazyme) referring to the protocols supplied by the manufacturer.

A murine intracranial glioma model and IHC analysis

16 male Bag albino (BALB)/c nude mice (4 weeks old) were purchased from the Shanghai Experimental Animal Center of the Chinese Academy of Sciences. pGBM-1 cells stably expressing luciferase were transfected with lentiviral vector LV-shcMELK or LV-shCONT, and then mice were subdivided randomly into an cMELK low-expression group and control group. To establish the intracranial GBM model, we implanted each mouse stereotactically with pGBM-1/luciferase+shcMELK or pGBM-1/luciferase+ shCONT (5×10^5) in each group. Intracranial tumor growth was measured by bioluminescence imaging. Each mouse was anesthetized and then given an intraperitoneal injection of D-luciferin (50 mg/mL). Tumors were imaged by means of the Living Image software package (Caliper Life Science, Waltham, MA, USA). Mouse survival time was monitored until the final mouse died. IHC analysis was performed to quantify proteins Vimentin, MMP2, and SOX2 in each brain tissue section. All the animal experiments were approved in accordance with the Animal Use Guidelines of the Chinese Ministry of Health (documentation 55,2001).

Statistical analysis

All the experiments were conducted in triplicate. All statistical analyses and Kaplan-Meier survival analysis were performed in GraphPad Prism 7.0 (GraphPad Software, San Diego, CA, USA). The correlation between circMELK expression and miR-593 levels in glioma tissues was evaluated by Pearson's correlation analysis. Two-tailed Student's t test was performed for other comparisons, and the results are expressed as the mean \pm standard deviation. Data with $p < 0.05$ were considered statistically significant.

SUPPLEMENTAL INFORMATION

Supplemental information can be found online at <https://doi.org/10.1016/j.omtn.2021.05.002>.

ACKNOWLEDGMENTS

This work was supported by grants from the National Natural Science Foundation of China (81672501 and 81872058), Jiangsu Province's Key Discipline of Medicine(ZDXKA2016001), and the Priority Academic Program Development of Jiangsu Higher Education Institutions (PAPD). We would like to thank the Core Facility of the First Affiliated Hospital of Nanjing Medical University for its help in the detection of experimental samples.

AUTHOR CONTRIBUTIONS

N.L. and H.Z. conceived and designed the experiments. F.Z., B.W., H.W., and L.H. performed the experiments. F.Z. wrote the paper. T.Y., X.X., J.Z., W.T., and C.Z. reviewed the manuscript. All authors reviewed the paper.

DECLARATION OF INTERESTS

The authors declare no competing interests.

REFERENCES

- Ostrom, Q.T., Gittleman, H., de Blank, P.M., Finlay, J.L., Gurney, J.G., McKean-Cowdin, R., Stearns, D.S., Wolff, J.E., Liu, M., Wolinsky, Y., et al. (2016). American Brain Tumor Association Adolescent and Young Adult Primary Brain and Central Nervous System Tumors Diagnosed in the United States in 2008-2012. *Neuro-oncol.* 18 (Suppl 1), i1–i50.
- Tanaka, S., Louis, D.N., Curry, W.T., Batchelor, T.T., and Dietrich, J. (2013). Diagnostic and therapeutic avenues for glioblastoma: no longer a dead end? *Nat. Rev. Clin. Oncol.* 10, 14–26.
- Mizumoto, M., Yamamoto, T., Ishikawa, E., Matsuda, M., Takano, S., Ishikawa, H., Okumura, T., Sakurai, H., Matsumura, A., and Tsuboi, K. (2016). Proton beam therapy with concurrent chemotherapy for glioblastoma multiforme: comparison of nimustine hydrochloride and temozolomide. *J. Neurooncol.* 130, 165–170.
- Srivastava, C., Irshad, K., Dikshit, B., Chattopadhyay, P., Sarkar, C., Gupta, D.K., Sinha, S., and Chosdol, K. (2018). FAT1 modulates EMT and stemness genes expression in hypoxic glioblastoma. *Int. J. Cancer* 142, 805–812.
- Zhang, J., Cai, H., Sun, L., Zhan, P., Chen, M., Zhang, F., Ran, Y., and Wan, J. (2018). LGR5, a novel functional glioma stem cell marker, promotes EMT by activating the Wnt/ β -catenin pathway and predicts poor survival of glioma patients. *J. Exp. Clin. Cancer Res.* 37, 225.
- Liu, Z.J., Liu, H.L., Zhou, H.C., and Wang, G.C. (2016). TIPE2 Inhibits Hypoxia-Induced Wnt/ β -Catenin Pathway Activation and EMT in Glioma Cells. *Oncol. Res.* 24, 255–261.
- Chen, J., McKay, R.M., and Parada, L.F. (2012). Malignant glioma: lessons from genomics, mouse models, and stem cells. *Cell* 149, 36–47.
- Cuddapah, V.A., Robel, S., Watkins, S., and Sontheimer, H. (2014). A neurocentric perspective on glioma invasion. *Nat. Rev. Neurosci.* 15, 455–465.
- Kahlert, U.D., Nikkhah, G., and Maciaczyk, J. (2013). Epithelial-to-mesenchymal(-like) transition as a relevant molecular event in malignant gliomas. *Cancer Lett.* 331, 131–138.
- Nakano, I. (2015). Stem cell signature in glioblastoma: therapeutic development for a moving target. *J. Neurosurg.* 122, 324–330.
- Wang, Z., Zhang, S., Siu, T.L., and Huang, S. (2015). Glioblastoma multiforme formation and EMT: role of FoxM1 transcription factor. *Curr. Pharm. Des.* 21, 1268–1271.
- Hansen, T.B., Jensen, T.I., Clausen, B.H., Bramsen, J.B., Finsen, B., Damgaard, C.K., and Kjems, J. (2013). Natural RNA circles function as efficient microRNA sponges. *Nature* 495, 384–388.
- Guo, J.U., Agarwal, V., Guo, H., and Bartel, D.P. (2014). Expanded identification and characterization of mammalian circular RNAs. *Genome Biol.* 15, 409.
- Shang, Q., Yang, Z., Jia, R., and Ge, S. (2019). The novel roles of circRNAs in human cancer. *Mol. Cancer* 18, 6.

15. Zhong, Z., Huang, M., Lv, M., He, Y., Duan, C., Zhang, L., and Chen, J. (2017). Circular RNA MYLK as a competing endogenous RNA promotes bladder cancer progression through modulating VEGFA/VEGFR2 signaling pathway. *Cancer Lett.* *403*, 305–317.
16. He, R., Liu, P., Xie, X., Zhou, Y., Liao, Q., Xiong, W., Li, X., Li, G., Zeng, Z., and Tang, H. (2017). circGFRA1 and GFRA1 act as ceRNAs in triple negative breast cancer by regulating miR-34a. *J. Exp. Clin. Cancer Res.* *36*, 145.
17. Du, W.W., Yang, W., Liu, E., Yang, Z., Dhaliwal, P., and Yang, B.B. (2016). Foxo3 circular RNA retards cell cycle progression via forming ternary complexes with p21 and CDK2. *Nucleic Acids Res.* *44*, 2846–2858.
18. Yang, Z.G., Awan, F.M., Du, W.W., Zeng, Y., Lyu, J., Wu, D., Gupta, S., Yang, W., and Yang, B.B. (2017). The Circular RNA interacts with STAT3, Increasing Its Nuclear Translocation and Wound Repair by Modulating Dnmt3a and miR-17 Function. *Mol. Ther.* *25*, 2062–2074.
19. Smid, M., Wilting, S.M., Uhr, K., Rodríguez-González, F.G., de Weerd, V., Prager-Van der Smissen, W.J.C., van der Vlugt-Daane, M., van Galen, A., Nik-Zainal, S., Butler, A., et al. (2019). The circular RNome of primary breast cancer. *Genome Res.* *29*, 356–366.
20. Liu, F., Zhang, H., Xie, F., Tao, D., Xiao, X., Huang, C., Wang, M., Gu, C., Zhang, X., and Jiang, G. (2020). Hsa_circ_0001361 promotes bladder cancer invasion and metastasis through miR-491-5p/MMP9 axis. *Oncogene* *39*, 1696–1709.
21. Cheng, Z., Yu, C., Cui, S., Wang, H., Jin, H., Wang, C., Li, B., Qin, M., Yang, C., He, J., et al. (2019). circTP63 functions as a ceRNA to promote lung squamous cell carcinoma progression by upregulating FOXM1. *Nat. Commun.* *10*, 3200.
22. Chen, J., Chen, T., Zhu, Y., Li, Y., Zhang, Y., Wang, Y., Li, X., Xie, X., Wang, J., Huang, M., et al. (2019). circPTN sponges miR-145-5p/miR-330-5p to promote proliferation and stemness in glioma. *J. Exp. Clin. Cancer Res.* *38*, 398.
23. Zheng, J., Liu, X., Xue, Y., Gong, W., Ma, J., Xi, Z., Que, Z., and Liu, Y. (2017). TTBK2 circular RNA promotes glioma malignancy by regulating miR-217/HNF1 β /Derlin-1 pathway. *J. Hematol. Oncol.* *10*, 52.
24. Mann, F., Peuckert, C., Dehner, F., Zhou, R., and Bolz, J. (2002). Ephrins regulate the formation of terminal axonal arbors during the development of thalamocortical projections. *Development* *129*, 3945–3955.
25. Flanagan, J.G., and Vanderhaeghe, P. (1998). The ephrins and Eph receptors in neural development. *Annu. Rev. Neurosci.* *21*, 309–345.
26. Kania, A., and Klein, R. (2016). Mechanisms of ephrin-Eph signalling in development, physiology and disease. *Nat. Rev. Mol. Cell Biol.* *17*, 240–256.
27. Wang, S.D., Rath, P., Lal, B., Richard, J.P., Li, Y., Goodwin, C.R., Lattera, J., and Xia, S. (2012). EphB2 receptor controls proliferation/migration dichotomy of glioblastoma by interacting with focal adhesion kinase. *Oncogene* *31*, 5132–5143.
28. Nakada, M., Niska, J.A., Tran, N.L., McDonough, W.S., and Berens, M.E. (2005). EphB2/R-Ras signaling regulates glioma cell adhesion, growth, and invasion. *Am. J. Pathol.* *167*, 565–576.
29. Wang, R., Zhang, S., Chen, X., Li, N., Li, J., Jia, R., Pan, Y., and Liang, H. (2018). EIF4A3-induced circular RNA MMP9 (circMMP9) acts as a sponge of miR-124 and promotes glioblastoma multiforme cell tumorigenesis. *Mol. Cancer* *17*, 166.
30. Zhong, S., Wang, J., Zhang, Q., Xu, H., and Feng, J. (2018). CircPrimer: a software for annotating circRNAs and determining the specificity of circRNA primers. *BMC Bioinformatics* *19*, 292.
31. Jeck, W.R., and Sharpless, N.E. (2014). Detecting and characterizing circular RNAs. *Nat. Biotechnol.* *32*, 453–461.
32. Okolie, O., Bago, J.R., Schmid, R.S., Irvin, D.M., Bash, R.E., Miller, C.R., and Hingtgen, S.D. (2016). Reactive astrocytes potentiate tumor aggressiveness in a murine glioma resection and recurrence model. *Neuro-oncol.* *18*, 1622–1633.
33. Bao, S., Wu, Q., Sathornsumetee, S., Hao, Y., Li, Z., Hjelmeland, A.B., Shi, Q., McLendon, R.E., Bigner, D.D., and Rich, J.N. (2006). Stem cell-like glioma cells promote tumor angiogenesis through vascular endothelial growth factor. *Cancer Res.* *66*, 7843–7848.
34. Wakimoto, H., Kesari, S., Farrell, C.J., Curry, W.T., Jr., Zaupa, C., Aghi, M., Kuroda, T., Stemmer-Rachamimov, A., Shah, K., Liu, T.C., et al. (2009). Human glioblastoma-derived cancer stem cells: establishment of invasive glioma models and treatment with oncolytic herpes simplex virus vectors. *Cancer Res.* *69*, 3472–3481.
35. Galli, R., Binda, E., Orfanelli, U., Cipelletti, B., Gritti, A., De Vitis, S., Fiocco, R., Foroni, C., Dimeco, F., and Vescovi, A. (2004). Isolation and characterization of tumorigenic, stem-like neural precursors from human glioblastoma. *Cancer Res.* *64*, 7011–7021.
36. Zarkoob, H., Taube, J.H., Singh, S.K., Mani, S.A., and Kohandel, M. (2013). Investigating the link between molecular subtypes of glioblastoma, epithelial-mesenchymal transition, and CD133 cell surface protein. *PLoS ONE* *8*, e64169.
37. Wang, Y., and Jiang, T. (2013). Understanding high grade glioma: molecular mechanism, therapy and comprehensive management. *Cancer Lett.* *331*, 139–146.
38. Jin, P., Huang, Y., Zhu, P., Zou, Y., Shao, T., and Wang, O. (2018). CircRNA circHIPK3 serves as a prognostic marker to promote glioma progression by regulating miR-654/IGF2BP3 signaling. *Biochem. Biophys. Res. Commun.* *503*, 1570–1574.
39. Peng, H., Qin, C., Zhang, C., Su, J., Xiao, Q., Xiao, Y., Xiao, K., and Liu, Q. (2019). circCPA4 acts as a prognostic factor and regulates the proliferation and metastasis of glioma. *J. Cell. Mol. Med.* *23*, 6658–6665.
40. Chen, M., Liu, X., Xie, P., Wang, P., Liu, M., Zhan, Y., Wang, H., Feng, Y., and Li, Y. (2020). Circular RNA circ_0074026 indicates unfavorable prognosis for patients with glioma and facilitates oncogenesis of tumor cells by targeting miR-1304 to modulate ERBB4 expression. *J. Cell. Physiol.* *235*, 4688–4697.
41. Han, D., Li, J., Wang, H., Su, X., Hou, J., Gu, Y., Qian, C., Lin, Y., Liu, X., Huang, M., et al. (2017). Circular RNA circMTO1 acts as the sponge of microRNA-9 to suppress hepatocellular carcinoma progression. *Hepatology* *66*, 1151–1164.
42. Nakada, M., Niska, J.A., Miyamori, H., McDonough, W.S., Wu, J., Sato, H., and Berens, M.E. (2004). The phosphorylation of EphB2 receptor regulates migration and invasion of human glioma cells. *Cancer Res.* *64*, 3179–3185.
43. Lin, L., Chen, X., Peng, X., Zhou, J., Kung, H.F., Lin, M.C., and Jiang, S. (2013). MicroRNA-128 promotes cell-cell adhesion in U87 glioma cells via regulation of EphB2. *Oncol. Rep.* *30*, 1239–1248.
44. Ying, Z., Li, Y., Wu, J., Zhu, X., Yang, Y., Tian, H., Li, W., Hu, B., Cheng, S.Y., and Li, M. (2013). Loss of miR-204 expression enhances glioma migration and stem cell-like phenotype. *Cancer Res.* *73*, 990–999.
45. Chen, X., Zhang, D., Wang, Y., Chen, K., Zhao, L., Xu, Y., Jiang, H., and Wang, S. (2020). Synergistic antifibrotic effects of miR-451 with miR-185 partly by co-targeting EphB2 on hepatic stellate cells. *Cell Death Dis.* *11*, 402.
46. Duan, S., Wu, A., Chen, Z., Yang, Y., Liu, L., and Shu, Q. (2018). miR-204 Regulates Cell Proliferation and Invasion by Targeting EphB2 in Human Cervical Cancer. *Oncol. Res.* *26*, 713–723.